Structure of the Amorphous Phase in Oriented Polymers

N. S. Murthy,* H. Minor, and C. Bednarczyk

Research and Technology, Allied-Signal Inc., Morristown, New Jersey 07962

S. Krimm

Department of Physics, University of Michigan, Ann Arbor, Michigan 48109

Received October 6, 1992; Revised Manuscript Received December 28, 1992

ABSTRACT: Changes in the position, width, and shape of the amorphous halo with orientation in the X-ray diffraction patterns of amorphous and semicrystalline polymers are used to study the medium-range order in the amorphous phase. Analysis of the data shows that a fraction of the amorphous domains is preferentially oriented. The chain segments in these domains are more densely packed, and these changes in density are accompanied by changes in the conformation of the polymer chains. The variations in the amorphous scattering are simulated by varying the density of packing of a two-dimensional assembly of hard disks. The diameter of such a disk is ~4.3 Å for polyethylene, which is larger than the Lennard-Jones diameter of 3.9–4.1 Å. In polymers such as nylons and polyesters, the molecular packing is determined by varying contributions of more than one interchain interaction. The medium-range order in such oriented amorphous regions seems to arise from the same interactions that determine the crystal structure.

Introduction

The importance of the structure of the amorphous phase was stated succinctly by Flory when he wrote that progress toward understanding the physical properties of polymeric materials cannot occur until issues concerning spatial conformation and intermolecular packing of polymer chains in the amorphous phase are resolved.[1] The structure of the amorphous phase reflects the thermomechanical history of a polymer and is important for understanding the mechanism of crystallization and in describing the correlation between the morphology and properties of the polymer. Mechanical properties such as modulus, tenacity, and yield point in fibers, permeability to oxygen, water vapor and various other gases through films, toughness of plastics, and dimensional stability of polymers in general are just a few examples of properties which depend directly on the structure of the amorphous phase. In spite of the difficulties, many workers have attempted to unravel the organization of the polymer chains in the amorphous phase. As noted by Katz more than 60 years ago, there is great uncertainty in the conclusions pertaining to the amorphous structure of a polymer, but the true picture can be approximated by a careful examination of the available data.[2]

We use the term amorphous to identify structures which do not have long-range three-dimensional order. The term noncrystalline also implies absence of such order, but this includes materials such as liquid crystals which possess one-dimensional and two-dimensional long-range order.[3] By definition, the amorphous phase cannot be described precisely. At one extreme, according to Bernal, the short-range order in the amorphous phase bears no resemblance to the crystalline order.[4] At another extreme, according to Hosemann, the amorphous phase is the result of paracrystalline distortions in the crystal lattice.[5] In describing oriented polymers, however, the range of possible models is probably limited, and in this case it should be possible to arrive at a useful working model of the amorphous phase that is consistent with the available data.

The "coil" and the "bundle" models are often used in discussing amorphous structure in polymers. In the random-coil model of Flory, the flexible chains in the amorphous phase assume unperturbed random spatial conformations corresponding to those for the same polymer in a Θ-solvent.[1] This model is supported primarily by the data of Benoit[6] and Wignall et al.,[7] who found that the radius of gyration in the solid state is the same as that in a Θ-solvent. But in many cases the radius of gyration is not much affected by crystallization.[8] According to the bundle model of Kargin,[9] Geil,[10] Yeh,[11] and others, amorphous polymers consist of small domains (30–100 Å) in which there is some degree of short-range order or alignment of the neighboring chains. This model derives primarily from electron microscopic observations. Although Fischer earlier found that the near-range order in amorphous polymers cannot be described by the assumption of a parallel packing of neighboring chains,[12] he has recently shown that medium-range ordering or clustering is possible.[13] In this paper we extend this work and use X-ray diffraction (XRD) results to explore the extent of medium-range ordering in oriented polymers.

Amorphous polymers, and amorphous components in semicrystalline polymers, give rise to diffuse X-ray scattering. This diffuse halo splits into equatorial arcs when the polymer chains are oriented, as shown in 1936 by Katz using stretched polystyrene.[2] Ruland in 1967 observed a similar anisotropic intensity distribution even in semicrystalline nylons[14] and concluded that at least some of the amorphous domains are anisotropic and preferentially oriented.[3] XRD data from stretched rubber obtained by Ohlberg et al. in 1954 show that the maximum in the amorphous scattering along the equator occurs at a slightly higher angle than along the meridian.[15] Earlier, in 1951, Krimm and Tobolsky noticed the differences in the position of the amorphous halo in the equatorial and meridional directions in oriented polystyrene.[16] The data from rubber suggest that the amorphous chain segments oriented parallel to the draw directions are packed more densely than those oriented perpendicular to the draw direction. We have published preliminary results which show that the amorphous density changes with orientation even in semicrystalline polymers.[17,18]

* To whom correspondence should be addressed.

0024-9297/93/2226-1712$04.00/0

In this paper, we present an analysis of the amorphous scattering in amorphous and semicrystalline polymers using the data from polystyrene (PS), polyethylene (PE), poly(ethylene terephthalate) (PET),[17] nylon 6 (N6),[18-22] and nylon 4,6 (N4,6).[23] We analyze the azimuthal variations in the intensity distribution in the amorphous halo and evaluate amorphous orientation in terms of the degree of orientation and fractional orientation. We also analyze the radial intensity distribution of the first major peak in the amorphous scattering and relate it to the lateral order or packing density of the amorphous chain segments. The scattering perpendicular to the chain axis is calculated by approximating the polymer chains in projection as disks. We discuss the implication of these results for the structure of the amorphous phase and show that the amorphous chain conformation varies with packing density and that the interchain structure bears some resemblance to the crystalline structure.

Materials and Methods

Polystyrene (MW 280 000; Aldrich) was molded into a 10-mil-thick film, drawn 3× at 100 °C, and quickly quenched in the drawn state using dry CO_2. A high-density PE film blow-molded from Allied-Signal's 4107 resin (melt index 0.96) was drawn to breaking (8×) at 100 °C. Commercially produced N6 yarn (formic acid viscosity 85, $M_n \sim 35\,000$) was annealed at 150 °C to eliminate the residual γ form. N4,6 monofilaments (Johnson Filaments) were produced from the resin obtained from DSM and were annealed under constraint at 150 °C in dynamic vacuum.

Radial XRD scans at various azimuthal angles were obtained on a Philips diffractometer in transmission geometry and slit collimation using copper radiation and a diffracted beam monochromator. Equatorial and meridional scans from PS were obtained on a Huber diffractometer using copper radiation with a incident beam focusing monochromator and pinhole collimation. Profile analysis of these scans was carried out using a modified version of the Program SHADOW.[24,25] After analyzing diffraction scans of a variety of samples on the Philips diffractometer, we chose a modified Lorentzian ($I = I_0/(1 + kx^2)^2$; $k = 0.4142/(\text{fwhm}/2)^2$, fwhm being the full width at half-maximum) to describe peak shapes since this gave the best fit with the least number of parameters.

Results

The equatorial and meridional scans of the drawn atactic PS film are shown in Figure 1. The best possible curve through the observed points was obtained using a minimum number of parameters (two broad peaks at $2\theta \sim 10°$ and 19° for both scans and an additional narrower peak at ~19° for the meridional scan). The low-angle peak shifts from 10.31° on the equator to 9.84° on the meridian. The high-angle peak shifts in the opposite direction, from 18.97° on the equator to 19.65° on the meridian. The first peak at ca. 10° has a d-spacing of 8.9 Å in unoriented PS and 8.6 and 9.0 Å along the equator and the meridian, respectively, in oriented PS. This is opposite to that observed by Krimm and Tobolsky based on more limited data.[16] The second peak at ca. 19° is at 4.60 Å in unoriented PS and shifts to 4.68 and 4.50 Å along the equator and the meridian, respectively, in oriented PS. These values are in agreement with the values of 4.67 and 4.57 Å reported by Krimm and Tobolsky.[16]

Profile-fitted radial scans of drawn PE film obtained at four representative azimuthal angles (ϕ) are shown in Figure 2. The changes in the intensities of the crystalline peak (110 reflection) and the amorphous halo with the azimuthal angle are shown in parts a and b of Figure 3, respectively. The amorphous halo along the equator is narrower and occurs at slightly higher angles than along the meridian. These variations in the position and the width of the amorphous halo with the azimuthal angle are

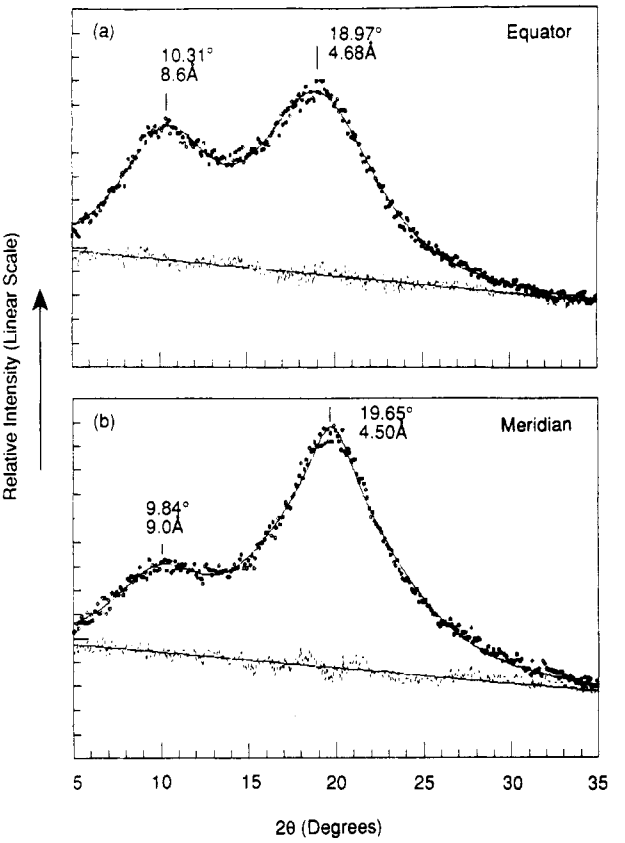

Figure 1. Equatorial (a) and meridional (b) scans of oriented atactic polystyrene (drawn 3× at 100 °C and quick quenched). The observed data (filled circles) are fitted to the curve shown by the full line. The difference between the observed data and the fitted curve is shown by the dashed line around the base line (full line).

plotted in parts c and d of Figure 3, respectively. The crystalline peaks in PE are very intense relative to the amorphous halo along the equator. Therefore, artifacts (see Analysis) which contribute to the tails of the crystalline peak are larger in PE than in other polymers such as N6 and PET. If this is the case, then the range of variations in the position, height, and width of the amorphous peak will be smaller than those shown in parts b–d of Figure 3. These changes are probably ca. 10%, as estimated by fitting a braod second peak to account for the tails of the crystalline peaks.

Figure 4 shows the radial scans from a drawn high-α N6 fiber at various azimuthal angles. The profile analysis of some these scans is illustrated in Figure 5. The results of these profile analyses are summarized in Figure 6. The position of the amorphous halo depends on the azimuthal angle; it changes from $2\theta \sim 20°$ (d = 4.44 Å) near the meridian to $2\theta \sim 21.5°$ (d = 4.13 Å) near the equator. Furthermore, the width, $\Delta 2\theta$, of the amorphous halo is smallest (4°) along the equator and reaches a maximum (6°) along the meridian. These are the average values (1 standard deviation is 0.2°) calculated from 10 recently analyzed commercial fibers containing both the α and γ crystalline forms. The results from the various fibers are summarized in Table I.

Additional XRD data are shown in Figures 7–9 to further aid in understanding the relationship between the diffuse scattering and the amorphous structure. Profile-fitted XRD scans of a N4,6 monofilament are presented in Figure 7. As in the case of PS, PE, and N6, the amorphous halo occurs at a higher angle on the equator than along the meridian (21.8–22.7° vs 20.5°). XRD photographs of a biaxially oriented N6 film, and the chain orientation

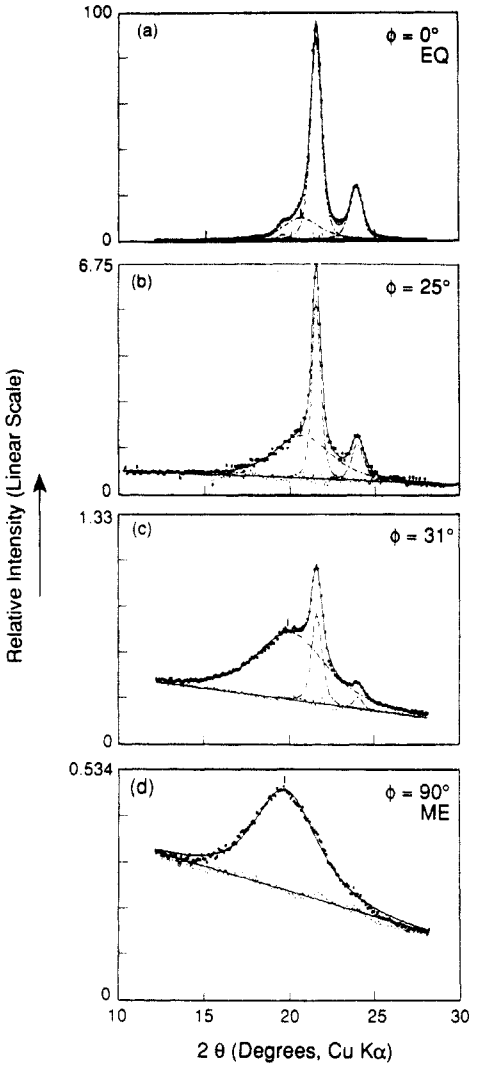

Figure 2. Profile-fitted radial XRD scans of a drawn polyethylene film at the azimuthal angles indicated next to each of the scans. In these and other profile-fitted scans, the filled circles are the observed intensities; the broken lines are the resolved components; the full line through the circles is the sum of the resolved components; the base line is shown by a full line; and the dotted line near the base line is the difference between the observed and the fitted intensities.

deduced from these photographs, are given in Figure 8. Transmission scans of the biaxial film with X-rays incident along the normal and transverse directions of the film, N- and T-scans, respectively, are given in Figure 9. The amorphous halos in the normal scan and the transverse scan (equivalent to a parafocus scan) are at ~21° and ~22°, respectively, and are slightly offset relative to the positions of the α_1 and the α_2 peaks.

Analysis

The positions of the peak maxima (2θ) in the amorphous scattering are convenient for identifying the peaks and the d-spacing of the peaks, $d = \lambda/(2 \sin \theta)$, and provide an "order of magnitude of the distance of closest approach" of the scattering entities.[26] The preferred method of analyzing the diffuse halo is via a radial distribution function. However, it is often necessary to evaluate the amorphous scattering in the reciprocal space rather than in real space, such as for calculating a degree of crystallinity and correct intensities for structure determination. Furthermore, although information on the molecular structure is more directly accessible in the radial distribution function, the intensity distributions give a clearer picture of the intermolecular arrangements.[3] Over the past few years we have been attempting to understand the factors which influence the amorphous scattering in the reciprocal space.[17,18,25]

Before we can analyze the amorphous halo, we have to understand the contribution of thermal diffuse scattering (TDS, which also includes disorder of the first kind) to the diffuse halo. It is difficult, perhaps impossible, to separate the TDS from amorphous scattering. But we can estimate the relative contributions of TDS and amorphous scattering by examining the off-equatorial scans (e.g., Figures 2b,c and 5b). The crystalline orientation is usually higher than the average amorphous orientation. Therefore, the decrease in the intensities of the crystalline peaks with the azimuthal angle is faster than that of the diffuse halo. Since the TDS is proportional to the intensity of the crystalline peaks, if the diffuse halo had a significant contribution from TDS, then it would be considerably weaker off the equator. This is contrary to what is observed, and hence the TDS contribution to the diffuse halo must be small compared to the scattering from the amorphous phase. Additionally, farther away from the equator, where the crystalline peaks are almost absent, the diffuse intensity is what one would expect from a Gaussian distribution of the orientation of the amorphous chain segments (Figures 3b and 6a). Thus, TDS does not constitute a large fraction of the diffuse scattering.

It might be possible to argue that the diffuse halo along the meridian in N6 (Figure 5c) is due to TDS of the crystalline peak (040) at $2\theta = 20.3°$, because the position of the meridional halo in an α-rich fiber (fiber axis repeat $b = 17.2$ Å) coincides with the position of the 040 crystalline peak. However, in N4,6, in which the crystalline form has a fiber axis repeat $b = 14.8$ Å, the amorphous halo remains essentially in the same position, while the 040 crystalline peak occurs at a much higher angle and hence is offset from the meridional halo (Figure 7). Such data enable us to rule out the possibility that the broad halo along the meridian in the α form of N6 is largely due to TDS underneath the 040 reflection.

Based on the above considerations, as a first approximation we attribute the diffuse halo at all azimuthal angles entirely to scattering from the amorphous regions. Detailed line-shape analysis, which requires data with counting statistics better than what we presently have, is necessary before we can attempt to separate the weak TDS contribution from the amorphous scattering. By ignoring TDS we will be overestimating the heights of the amorphous halo near the equator, and this can account for the lack of good fit near the tails in the amorphous intensity vs ϕ curve for PE (Figure 3b). Such errors do not appear to affect our conclusions regarding the orientation and the density of the amorphous phase.

Amorphous Orientation. The plots of the azimuthal intensity variations in the amorphous halo (Figures 3b and 6a) show an equatorial peak on a flat, nonzero, base line. The crystalline peaks, on the other hand, have an almost zero base line (Figures 3a and 6b,c).[18,27] The equatorial amorphous scattering is due to chain segments oriented parallel to the chain axis, and the meridional amorphous scattering is due to chain segments oriented perpendicular to the chain axis. The constant value of the base line suggests that the meridional scattering is largely due to randomly oriented chain segments. Thus, the intensity below the base line can be attributed to the unoriented, isotropic, amorphous component, and the intensity above the base line can be attributed to the oriented, anisotropic, amorphous component.[18,27,28]

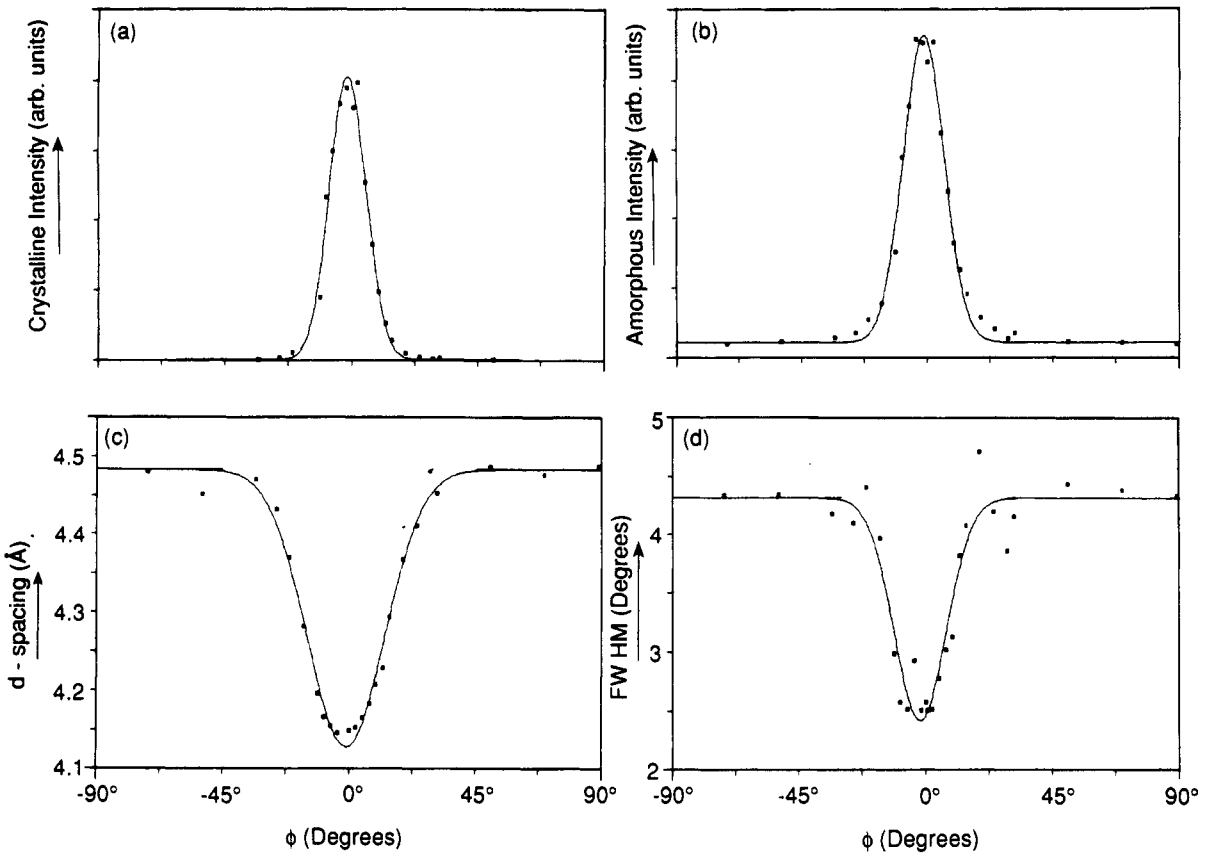

Figure 3. Summary of the profile analyses presented as plots of various peak parameters as a function of the azimuthal angle. (a) Crystalline (110) intensity. (b) Amorphous intensity. (c) *d*-Spacing of the amorphous halo. (d) Full width at half-maximum of the amorphous halo.

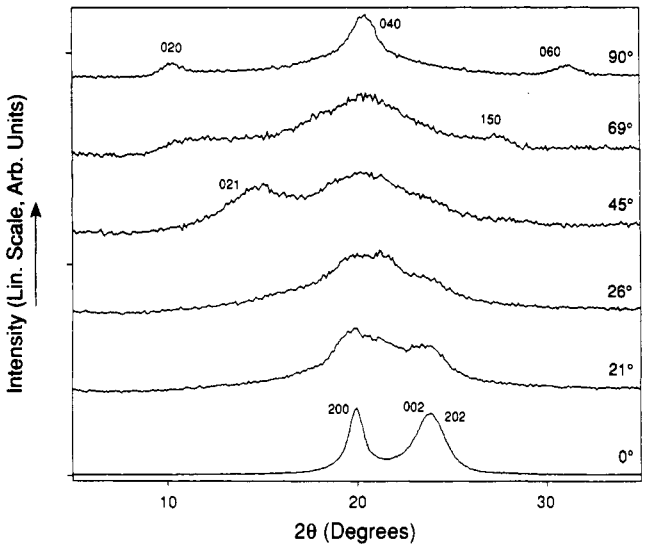

Figure 4. Radial XRD scans from a drawn high-α N6 fiber at the azimuthal angles indicated next to each curve: $\phi = 0°$, equator; $\phi = 90°$, meridian. The crystalline reflections are indicated by their Miller indices.

The crystalline orientation (Figures 3a and 6b,c) is usually described by a single parameter such as the degree of orientation (f_c) calculated from the width of the peak. However, it can be seen from the plots of $I(\phi)$ vs ϕ (Figures 3b and 6a) that two parameters are required to describe amorphous orientation. A parameter f_a, the degree of amorphous orientation, can be calculated from the width of the peak by analogy with crystalline orientation. A second parameter F_a, fractional amorphous orientation, defined as the area of the peak (after correction for the cylindrical symmetry of the oriented segments) normalized to the total area under the curve, is necessary to take into account the height of the nonzero base line. F_a is given by the expression

$$F_a = [\int_{-\pi/2}^{\pi/2} I_p(\phi) \cos\phi \, d\phi]/[(\int_{-\pi/2}^{\pi/2} I_p(\phi) \cos\phi \, d\phi) + \pi I_b] \quad (1)$$

where I_p and I_b are the peak and the base-line intensities, respectively. Data from N6 fibers show that processing steps such as drawing and annealing affect both f_a and F_a and that F_a greatly influences fiber properties such as strength, modulus, and shrinkage.[18]

In our analysis, we have not taken into account any second-order geometrical factors which affect the amorphous scattering. For instance, f_a is only an apparent degree of orientation because the azimuthal broadening of the reflections inherent in an array of parallel molecules is not taken into account. This requires deconvolution using cylindrical distribution functions. Further, we have not taken into account enhancement of the equatorial intensity by the interference function of the ordered amorphous chain segments oriented parallel to the fiber axis. There are essentially two models to describe the amorphous orientation. In one model, the orientation refers to the alignment of individual molecules. In the second model, which is implicit in the above calculations, the orientation refers to the orientation of aggregates of molecules, the molecules within the aggregate being in perfect alignment.

Amorphous Density. The changes in amorphous density are reflected in the changes in the widths and positions of the amorphous halo. This assumption is valid in the angular range in which the scattering is dominated by interchain scattering, which is typically between $2\theta = 5°$ and 35° with Cu Kα radiation. To understand the changes in the amorphous halo, we will initially approx-

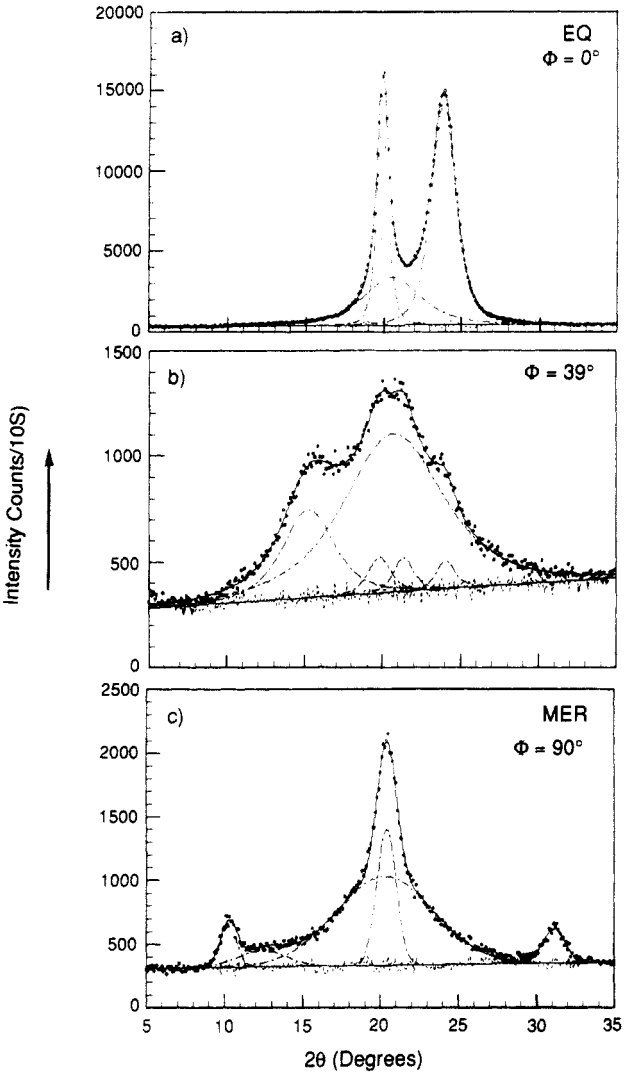

Figure 5. Typical profile-fitted radial scans of the sample used in Figure 4 at three azimuthal angles. (a) Equatorial. (b) Off-axis. (c) Meridional.

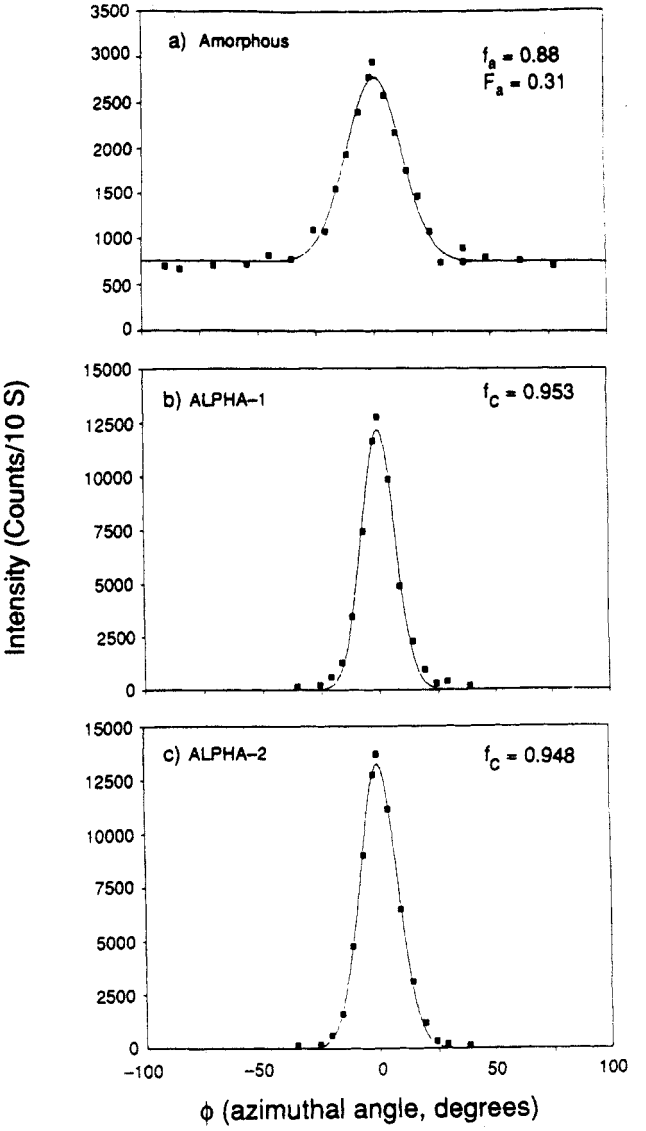

Figure 6. Plot of the amorphous and the crystalline intensities as a function of the azimuthal angle for the fiber used for Figure 5. The degree of crystalline orientation (f_c), the degree of amorphous orientation (f_a), and the fractional amorphous orientation (F_a) are given in the figure.

imate the chains in chain-axis projection as circular disks (implying that the orientations about the chain axes of the neighboring chains are uncorrelated). A two-dimensional assembly of such disks provides an adequate representation of the packing of the polymer molecules for calculating the equatorial scattering at intermediate scattering angles. Although the structure factors of the two-dimensional packing of disks can be calculated using Percus–Yevick approximations, we will use the analytical equations developed by Rosenfeld based on a free-energy model.[29]

The intensities $I(q)$ at $q = 4\pi \sin(\theta)/\lambda$, 2θ being the scattering angle, were computed using the expression[30]

$$I(q) = S(q)\, F^2(q) \tag{2}$$

where $S(q)$ is the interference function (also sometimes confusingly called the "structure factor"[29]) and $F(q)$ is the structure factor of a single chain. $F(q)$ was calculated from the Debye formula using the coordinates of the trans conformation of the ethylene segments using the expression

$$F(q) = \sum_m \sum_n (f_m f_n \sin qr_{mn})/(qr_{mn}) \tag{3}$$

in which f is the atomic scattering factor and r_{mn} is the distance between the mth and nth atoms in the chain in projection. The interference function $S(q)$ for an assembly of disks of diameter σ (=2a) at a packing density of η is given by the expression

$$S(q)^{-1} - 1 = 4\eta\{A[J_1(qa)/qa]^2 + BJ_0(qa)\, J_1(qa)/qa + GJ_1(2qa)/qa\} \tag{4}$$

where

$$A = [1 + (2\eta - 1)\chi + 2\eta G]/\eta \tag{5}$$

$$B = [(1 - \eta)\chi - 1 - 3\eta G]/\eta \tag{6}$$

$$G = 1/(1 - \eta)^{1.5} \tag{7}$$

$$\chi = (1 + \eta)/(1 - \eta)^3 \tag{8}$$

The factor $(1 + \eta)$ of eq 8 is printed erroneously as $(1 - \eta)$ in ref 29 (Rosenfeld, Y., private communication).

Examples of $I(2\theta)$ curves calculated using the above equations are shown in Figure 10. The full width at half-maximum of the amorphous halo and the d-spacing of the peak maximum of such curves were calculated for disks of various diameters and at several packing densities.

Table I
Comparison of the Amorphous and Crystalline Peak Positions in Various Nylon 6 Samples[a]

sample	H-bonded	van der Waals + H-bonded
	Oriented Amorphous Halo	
biaxial film	20.86 (4.26) N	22.33 (3.98) T
formic acid α	21.08 (4.21) M	22.62 (3.93) E
KI/I_2 γ	21.33 (4.17) M	21.53 (4.12) E
commercial α	20.27 (4.38) M	21.76 (4.08) E
commercial γ	20.00 (4.44) M	21.50 (4.13) E
	Unoriented Amorphous Halo	
Roldan's data[19]	20.93 (4.25) fresh	
	21.4 (4.15) aged	
our data[39]	21.0 (4.23) gel	
melt 222 °C[21]	20.1 (4.42)	
	Crystalline Peaks	
(average values)		
α	20.0 (4.44) α_1	24.0 (3.71) α_2
γ	21.5 (4.13) γ_1	22.3 (3.99) γ_2

[a] Positions are given in degrees, and the corresponding d-spacings in angstroms are given within parentheses. N, normal; M, meridional; T, transverse; E, equatorial. α_1, 200; α_2, 002 + 202; γ_1, 001; γ_2, 200 + 20$\bar{1}$.

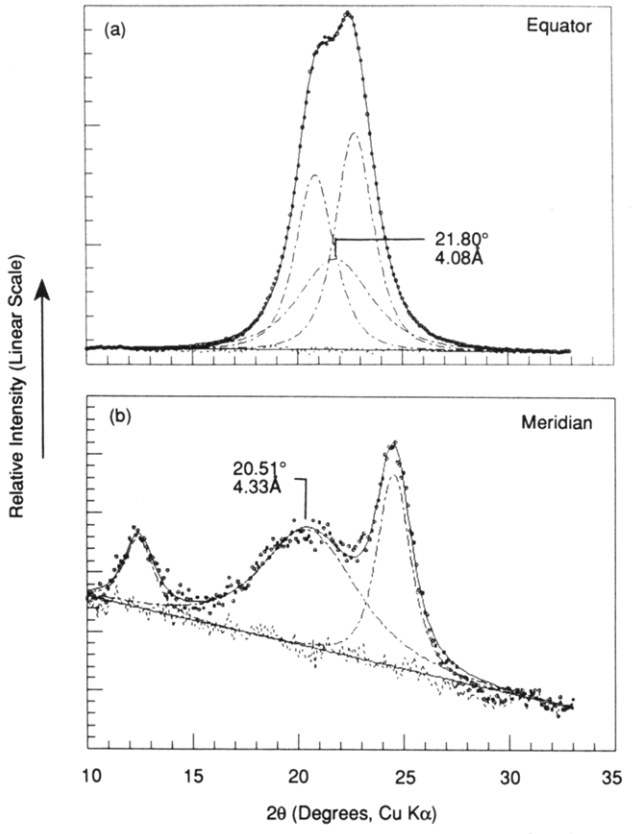

Figure 7. Profile-fitted radial scans of an oriented nylon 4,6 fiber. (a) Equatorial scan, perpendicular to the fiber axis. (b) Meridional scan, along the fiber axis.

Surprisingly, these points were found to define a grid with σ and η as the two axes (Figure 11). The diameters of 3.923 and 4.14 Å are the Lennard-Jones (LJ) repulsive soft-core diameters of the polymer chains predicted by the Anderson–Weeks–Chandler theory for PE using hard-core diameters of 3.70 and 3.90 Å, respectively.[31]

Discussion

While unconstrained flexible chains may indeed assume random-coil conformations, there is no reason to expect that chains under constraints behave the same way. Amorphous structure can be different depending on whether the polymer chains are under strain or not. The chains can be constrained because of orientation caused by drawing or by local stresses and internal constraints as they may occur at interfaces and between lamellae and fibrils in semicrystalline polymers. Inhomogeneous stress distributions which put the polymer chains under local strains are not uncommon. We discuss here the structure in oriented polymers and show that constraints such as

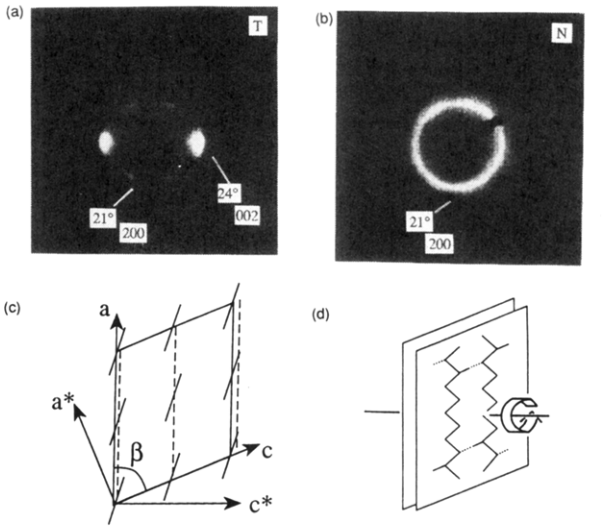

Figure 8. Transverse (a) and normal (b) photographs of a biaxially oriented N6 film. (c) Orientation of the unit cell in chain axis projection. (d) Orientation of the hydrogen-bonded chains relative to the plane of the film.

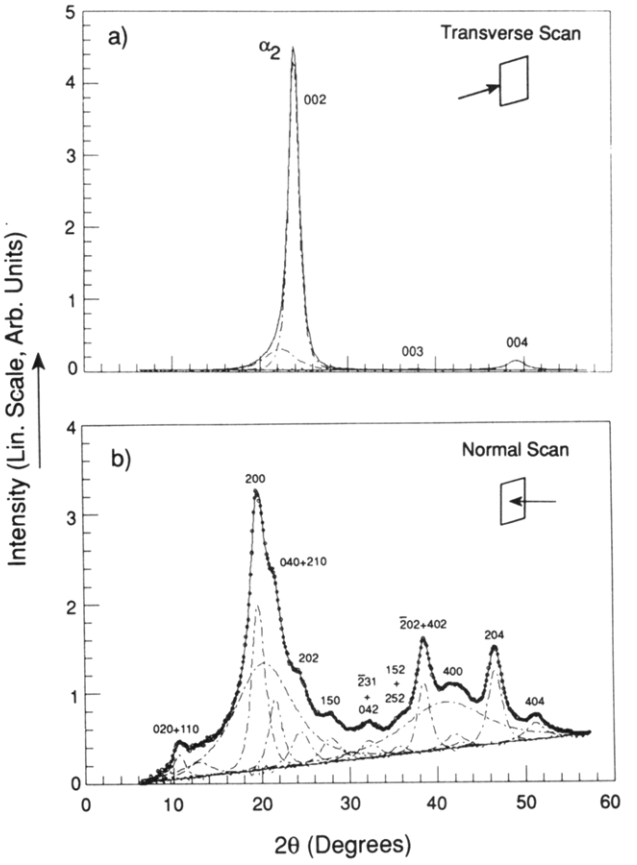

Figure 9. Transverse (a) and normal (b) diffractometer scans on a biaxial N6 film in transmission mode. Miller indices of some of significant crystalline reflections are indicated in the figure. Numerous 7th layer line reflections are not identified. The amorphous halos in the transverse and the normal scans are at 23.9° and 19.8°, respectively.

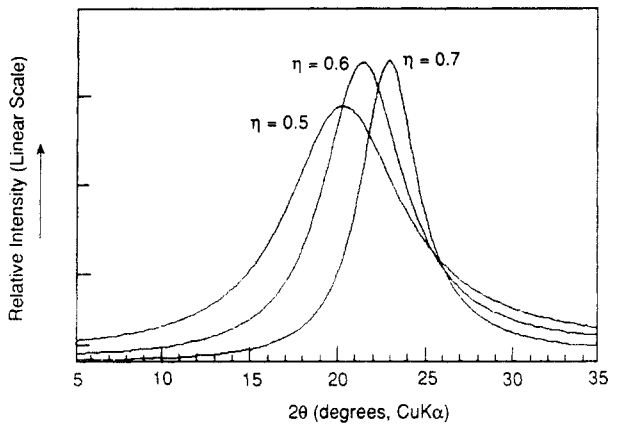

Figure 10. Calculated scattered intensities for a two-dimensional assembly of disks of diameter 3.923 Å at three packing densities, according to Rosenfeld.[29]

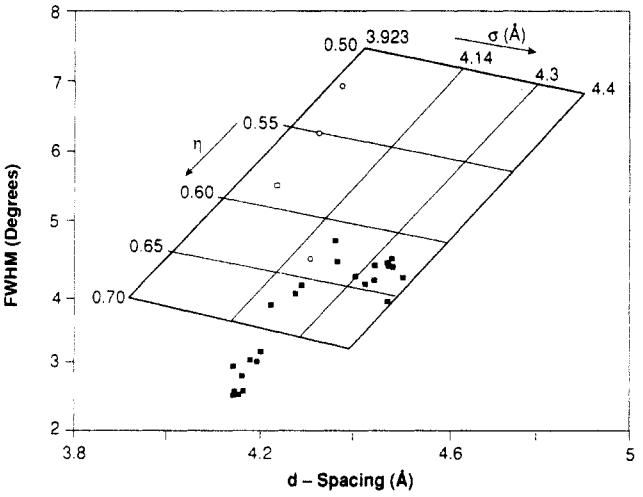

Figure 11. Width of the amorphous halo (fwhm) and the peak position (d-spacings) from PE and N6 plotted on a σ–η grid. The σ–η grid is drawn using the fwhm and the d-spacings of the amorphous halo calculated for disks of diameters 3.923, 4.14, 4.3, and 4.4 Å at packing fractions (η) of 0.5–0.7 in steps of 0.5. These points (not shown) fall at the intersection of the lines for constant diameter and constant density. Filled squares represent the values obtained at various azimuthal angles for the oriented HDPE film (Figures 2 and 3). The three open circles are the equatorial, off-axis, and meridional values of the amorphous halo for the N6 fiber used in Figures 4–6. The open square is from a quick-quenched (amorphous), unoriented N6 film.

these lead to medium-range ordering of the amorphous chain segments.

We have characterized amorphous orientation by separating the amorphous scattering into oriented and unoriented components. The question is, how are these two components physically distributed, particularly in a semicrystalline polymer? We suggest a general model in which the oriented components are mainly in the interfibrillar regions and the unoriented components are primarily in the lamellar stack within a fibril. This idea is consistent with our earlier conclusion based on the analysis of data from hydrated N6.[32] NMR data do not show nonlinear relaxation curves corresponding to two or more components (Curran, S. A., private communication). However, based on the equilibration of the relaxation rates by spin diffusion, the minimum detectable domain size in these NMR measurements is estimated to be ~40 Å. Since the amorphous scattering in XRD arises from interference between neighboring chains over a distance scale of 10–25 Å, the NMR results are not inconsistent with such a two-component model derived from the XRD results. It is, however, possible that such a physical separation into two components is only a conceptual tool and that F_a simply indicates the contribution of the amorphous chain segments to the scattering near the equator.

In oriented specimens, the amorphous halo corresponding to interchain distances occurs at higher angles along the equator than along the meridian (Figures 1–7 and Table I). This suggests that the chain segments oriented along the draw direction are packed more densely than those oriented perpendicular to the draw direction (and in general away from the equator) as well as the unoriented ones. The results of our calculation of the interchain scattering, assuming the polymer chains in projection as disks (Figures 10 and 11), show that the diffuse scattering can be related to the amorphous structure in terms of two parameters, the diameter of the polymer chain and the packing density. The plots in Figure 10 show that both the shift in the position of the amorphous halo to higher angles and the decrease in its width are due to an increase in the density of packing of the chains.

Polystyrene. The shift in the 10° (9 Å) amorphous halo to lower angles along the equator in drawn PS is not as pronounced as in rubber and is less than the shift to higher angles observed for the 19° (4.6 Å) peak (Figure 1). Failure to see these variations in d-spacing and azimuthal intensity (see ref 33) can be traced to high drawing temperatures. Molecular orientation can be obtained only when PS is drawn at temperatures of 100–105 °C (slightly above the T_g). At higher temperatures, PS can be stretched 7–8×, but the resulting orientation is mostly flow-induced and gives rise to form birefringence with very little molecular orientation.

Although we have identified the amorphous scattering from PS in Figure 1 by two d-spacings, more than one distance distribution function contributes to each of the two peaks. Wecker et al. have recently shown by radial distribution function analysis that about 87% of the contribution to the 4.6-Å peak comes from phenyl–phenyl interchain and phenyl–chain intrachain interactions.[34] Katz, back in 1936, noticed that liquid styrene shows the 4.6-Å ring and not the 9-Å "polymerization ring".[2] Furthermore, Killian and Boueke have shown that, at temperatures above the T_g (86 °C), the 9-Å peak moves to smaller angles whereas the 4.6-Å peak remains essentially unchanged.[35] On the basis of these observations, we can attribute the lower angle 9-Å peak to interchain distances and the higher angle 4.6-Å peak mainly to intrachain distances.[16] The shift in the interchain peak to higher angles along the equator suggests that the chains oriented parallel to the draw direction are more densely packed than those oriented perpendicular to it; the latter are packed about as densely as those in unoriented polymer. The shift in the intrachain peak to lower angles along the equator suggests that, as the chains move closer together upon drawing, their local conformation and therefore the orientation of the phenyl groups changes, so that the intrachain distances between the phenyl group and the main chain increase. The phenyl group might become more extended from the main chain as interchain distance decreases.

Polyethylene. The position, height, and width of the amorphous halo in the radial scans of PE depend strongly on how the profile analysis is done. There is no ambiguity in fitting the amorphous halo for $|\phi| > 20°$. But, while we find that the amorphous halo in equatorial (and near equatorial, $|\phi| < 20°$) scans occurs at $2\theta \approx 21°$, it has been customary to draw the amorphous halo at 19.5° (e.g., ref 36), primarily because of the ubiquitous "hump" to the

left of the 110 reflection. But this hump can be identified with the triclinic phase of PE[37] and thus does not provide the basis for positioning the amorphous halo. The scans just off the equator, in which the crystalline peaks are weak, clearly show that the amorphous halo in these scans (as well as on the equator) occurs at higher angles than along the meridian. Furthermore, attempts to fit the PE scans with other peak shapes, such as normal and intermediate Lorentzians with intense tails so as to fit part of the amorphous scattering and thus push the amorphous halo to lower angles on the equator, resulted in poor fits to the data and moved the amorphous halo to at most 20.5°. Finally, our choice of the position of the amorphous halo is substantiated by our observations in highly amorphous PE such as ionomers and cross-linked PE. As indicated by our profile analysis, the amorphous halo in the equatorial and near-equatorial scans in PE is at ca. 21.5°, higher than the 19.5° value found near the meridian. This shift is consistent with the shift in the amorphous peak to higher angles observed along the equator in PS, rubber, and nylons.

The widths and the d-spacings of the amorphous halo obtained from profile analysis of the radial scans at various azimuthal angles are superimposed on the σ–η grid in Figure 11. These points fall near the line calculated for a 4.3-Å-diameter disk. This is larger than the usually quoted 3.923 and 4.14 Å for the Lennard-Jones repulsive soft-core diameter of polyethylene.[31] It could be that, because of lack of perfect orientation, the chains should be treated in projection as elliptical rather than circular disks. The interaction between elliptical disks of different aspect ratios will increase the calculated diameter of the chains. Further, the chains may not be totally uncorrelated as in Rosenfeld's treatment (see the section Similarities between Amorphous and Crystalline Structures), and thus the disk diameter may not be directly identified with the physical dimensions of the chains.

The amorphous halos near the equator have smaller d-spacings than elsewhere around the azimuth and appear to correspond to densities higher than the density of 0.707 at freezing (i.e., at random close packing of disks; the density is 0.907 for the crystalline structure, i.e., ordered close-packed structures). This would imply that near-equatorial scattering arises from a "frozen" or dense amorphous phase. The similarity between the meridional halo and the amorphous halo in unoriented specimens suggests that either the meridional scattering is mostly due to randomly oriented chain segments (isotropic component) or that the distance between the amorphous chain segments oriented perpendicular to the chain axis is fortuitously the same as that in the isotropic, amorphous phase.

As in PS, the average conformations of the amorphous PE chain segments oriented perpendicular and parallel to the chain axis are expected to be different. This indication is substantiated by the IR data of Read and Stein.[38] They found that the dichroic ratio of the 1303-cm^{-1} amorphous band, associated with a mode whose transition moment is parallel to the chain axis, is smaller than the dichroic ratio of the 1368-cm^{-1} amorphous band, which is due to a structure with a transition moment of uncertain direction. It would be expected that, for oriented amorphous chains, the dichroic ratio of the 1303-cm^{-1} band should be higher. However, if the relative population of these two structures were different in chain segments oriented parallel and perpendicular to the fiber axis, the observed differences in dichroic ratios could occur.

Nylon 6. Data in Table I show that the position of the amorphous halo changes from 21.5–22.5° in the equatorial (uniax) or the transverse (biax) scans to 20–21° in the meridional (uniax) or normal (biax) scans. The half-width of the amorphous halo along the equator (transverse in a biax film) is ~4°, and this increases to 6–7° along the meridian (normal scans in a biax film). These changes are related to the changes in the packing density of the amorphous chain segments.

The width and position of the amorphous halo in N6 cannot be accurately determined from our currently available data because of the presence of layer lines (Figure 4). However, a comparison of the widths of the resolved peaks in Figure 5 with the calculated curves in Figure 10 suggests that the packing density increases from ~0.5 for chains oriented perpendicular to the chain axis to ~0.65 for the chains oriented parallel to the chain axis. The meridional values are similar to those obtained for unoriented N6. Average values of the full width at half-maximum of the amorphous halo of the scans near the equator and the meridian, as well as from several off-axis scans, are shown in Figure 11. Note that the LJ diameter corresponding to the hydrogen-bonded chains (meridional scans of oriented fibers and scans from quenched films) is ca. 4 Å, much less than the 4.3 Å found in our analysis for PE.

The crystalline regions in biaxial films are oriented such that the hydrogen-bonded (H-bonded) sheets are parallel to the plane of the film but are randomly oriented in this plane (Figure 8). The interference between the H-bonded sheets gives rise to the crystalline peak at 23.9° in the T-scan, and the separation between the H-bonded chains gives rise to the main peak at 19.8° in the N-scan (Figure 9). By comparing these crystalline peaks with the amorphous halos at 22.3° and 20.9° in the T- and N-scans, respectively, we conclude that the orientation of the amorphous chain segments is similar to those of the crystallites. Thus, the 20.9° halo in the N-scan corresponds to the average distance between the H-bonded chains, and the 22.3° halo in the T-scan, to the average van der Waals distances between non-H-bonded chains.

In a fiber in which the α form constitutes the entire crystalline fraction (formic acid treated fiber in Table I), the equatorial amorphous halo is at 22.6° (3.94 Å) and the meridional halo is at 21.1° (4.21 Å). The equatorial halo occurs at about the same angle as the amorphous peak in the transverse scan of the biaxial film. Hence, as in biaxial films, the equatorial amorphous halo is perhaps influenced largely by the interchain distances determined by the van der Waals interactions between H-bonded sheets. The meridional peak is similar to that obtained from a freshly quenched amorphous film[19] or an amorphous gel.[39] The similarity between the near-meridional scans of the fibers and the amorphous halo in the melt[21] (after we allow for thermal expansion) suggests that the packing of the randomly or perpendicularly oriented chains is close to that in the melt. The interchain distances contributing to the near-meridional scattering are perhaps determined, as in the melt, primarily by single-chain interactions.

The influence of the H-bonding interactions on the packing density is expected to be independent of the degree of intermolecular order, i.e., independent of orientation, temperature, coherence length, and whether the material is in the solid state or the melt. In contrast, the influence of the van der Waals interactions (of the type present in crystalline nylons) on the interchain distances is expected to be limited to relatively ordered aggregates of H-bonded chains, and therefore to increase with orientation and

decrease at elevated temperatures, and thus depend on the thermal and mechanical history of the sample. On the basis of NMR data, Miura et al. have suggested that there could be two subpopulations within the amorphous phase due to morphological and local constraints.[40] It could be that morphological constraints lead to ordered segments in which H-bonding between chains and nonbonded (van der Waals) interactions between H-bonded chains are present, and local constraints lead to disordered segments in which single-chain interactions prevail.

The packing density, and hence the relative contribution of nonbonded interactions, is affected by temperature, quenching rates, and annealing conditions, and this will be reflected in the shape and the position of the amorphous halo and in the densities of the various amorphous films. The shift in the amorphous halo to lower angles prior to melting[21] is a result of the decrease in packing density and suggests that melting is preceded by a decrease in the contributions of nonbonded interactions. The amorphous halo in N6 occurs at 20.7° in a freshly quenched film and at 21.4° in an aged amorphous film. Roldan referred to these amorphous states as fresh quenched states and stabilized quenched states.[19] It could be that only single-chain interactions are present in the fresh quenched state, and upon aging the amorphous phase is "stabilized" by additional van der Waals interactions between incipient H-bonded sheets.

The near-equatorial scattering in a N6 fiber arises from chains in which the packing is determined by both H-bonding and nonbonded interactions. Hence, the d-spacing of the near-equatorial amorphous peak is probably larger than if only van der Waals interactions were present, such as for instance in the transverse scan of a biax film. The meridional spacing in the commercial α fiber (which could contain a small amount of γ) is 0.1–0.2 Å larger than those of the two model α fibers, and the equatorial spacings in both commercial α and γ fibers are 0.1–0.2 Å larger than those of the three model fibers. Thus, when more than one crystalline form is present, the amorphous chains appear to be more loosely packed than if only the α or γ crystalline forms are present. On the basis of the data from PS and PE, we would expect the chains oriented parallel to the chain axis to be more extended (α-like) and the chains oriented perpendicular to the chain axis to be more collapsed (γ-like). This is consistent with the observation that the amorphous d-spacings along the equator are smaller than those along the meridian (Table I).

Similarities between Amorphous and Crystalline Structures. The above discussions lead us to propose a model in which the packing of the amorphous chain segments in any arbitrary N6 sample is determined by two contributions, the H-bonding interactions and the nonbonded or van der Waals interactions. These are the same interactions which determine the packing in the crystalline regions. In a γ fiber obtained by iodine treatment, the H-bonded and nonbonded (van der Waals) distances are not very different. This is similar to that observed in the γ crystal, which for all practical purposes is pseudohexagonal, suggesting that the amorphous structure follows the pattern set by the corresponding crystal structures.

Similarities between the amorphous order and the crystal structure can be found in PET also. In PET, it became necessary to describe the amorphous halo in the angular range of 5–35° by two amorphous peaks corresponding to the a^* and b^* distances (c being the chain axis) of the crystalline lattice.[17] On the basis of this observation, we suggested that there is some degree of spatial correlation, analogous to that in the crystalline regions, between the aromatic rings on neighboring PET chains. As in N6, we can describe this type of ordering in PET by two distance distribution functions, one due to dipole interactions and the other to nonbonded or π-electron interactions between the chains.

In contrast to N6 and PET, a single interchain distance distribution function is sufficient to describe the intensity distribution in the amorphous halo in PE. This is not surprising since PE chains in the crystalline state are known to exist in a disordered rotator phase.[41] This rotator phase, which only one type of nearest-neighbor interaction, could be considered as the crystalline analogue of the amorphous structure in PE.

The amorphous regions for which the diffuse halo is narrower than that in the melt can be described as a dense (or stabilized or condensed) amorphous phase. The amorphous phase whose scattering is similar to that of the melt can be described as a fluid amorphous phase. Highly oriented amorphous domains are examples of a stabilized amorphous phase, and amorphous domains in freshly quenched films are examples of a fluid amorphous phase. The results discussed earlier in this section indicate that the amorphous structure in a semicrystalline polymer can be regarded as a local representation of the long-range crystalline order. To the extent that local orientational correlations exist between neighboring chains in the amorphous phase, even in the simple case of polyethylene, the assumption of uncorrelated orientation of the neighboring chains, implicit in our use of Rosenfeld's treatment, would not be completely applicable. One consequence is that the disk diameters could not be interpreted in terms of the exact physical parameters of the polymer chain.

The difficulty of separating the amorphous halo at high packing densities (close to freezing) and TDS suggests that the dense amorphous phase may indeed be a disordered crystal lattice, and perhaps even similar to the paracrystalline lattice of Hosemann.[5] If this is the case, then an increase in the crystallinity would simply be a gradual increase in the crystalline order. This would be a second-order transition accompanied only by a decrease in the specific heat, somewhat analogous to the transition from a glassy to a rubbery state in the amorphous phase. Such a description of the condensed (i.e., stabilized) amorphous phase can at least partially explain the absence of a crystallization exotherm when a polymer with >30% of the maximum attainable crystallinity (e.g., 20% in N6) is heated in a differential scanning calorimeter even though there is an increase in the crystallinity. However, there are instances in which the amorphous phase is clearly a distinct disordered structure. In these cases, the increase in crystallinity is best described as a transformation from a fluid amorphous phase into a crystalline phase. This is a first-order transition and would be accompanied by a crystallization exotherm.

Conclusions. The structure in the amorphous phase in oriented polymers can be characterized by medium-range order and orientational anisotropy. Examination of the intensity distribution in the amorphous halos in polystyrene, polyethylene, and nylon 6 shows that the amorphous phase in oriented polymers is anisotropic and preferentially oriented. The amorphous orientation can be characterized by the fraction of the isotropic component and the degree of orientation of the anisotropic fraction. The oriented amorphous chain segments are more densely packed and probably adopt a conformation that is different from the less dense isotropic phase. The variation in

scattered intensity with packing density is simulated by assuming polymer chains in projection to be disks. Such a simulation shows that the diffuse scattering can be related to the amorphous structure in terms of two parameters, an equivalent diameter of the polymer chains and the packing density. The interchain interactions which determine the structure in the densely packed, anisotropic component are similar to those found in corresponding crystal structures. The structure in the less dense isotropic phase, referred to here as the fluid phase, is qualitatively not very different from that of the melt. It is possible that the crystallization behaviors of the dense or stabilized amorphous phase and the fluid phase are different, only the latter being accompanied by a crystallization exotherm.

Acknowledgment. We thank Dr. Y. Rosenfeld for helpful discussions of his paper[29] and Dr. K. Ding for discussions regarding correlation functions of model systems.

References and Notes

(1) Flory, P. J. *J. Macromol. Sci., Phys.* **1976**, *B12*, 1.
(2) Katz, J. R. *Trans. Faraday Soc.* **1936**, *32*, 77.
(3) Ruland, W. *Pure Appl. Chem.* **1969**, *18*, 489.
(4) Bernal, J. D. *Proc. R. Inst. G. B.* **1959**, *37*, 355.
(5) Hosemann, R.; Bagchi, S. N. *Direct Analysis of Diffraction by Matter*; North-Holland: Amsterdam, The Netherlands, 1962.
(6) Benoit, H. *J. Macromol. Sci., Phys.* **1976**, *B12*, 27.
(7) Wignall, G. D.; Ballard, D. G. H.; Schelten, J. *J. Macromol. Sci., Phys.* **1976**, *B12*, 75.
(8) Wendorff, J. H. *Polymer* **1982**, *23*, 543.
(9) Kargin, V. A. *J. Polym. Sci.* **1958**, *30*, 247.
(10) Geil, P. H. *J. Macromol. Sci., Phys.* **1976**, *B12*, 173.
(11) Yeh, G. S. *Pure Appl. Chem.* **1972**, *31*, 65.
(12) Fischer, E. W.; Wendorff, J. H.; Dettenmaier, M.; Lieser, G.; Voigt-Martin, I. *J. Macromol. Sci., Phys.* **1976**, *B12*, 41.
(13) Cervinka, L.; Fischer, E. W. *J. Non-Cryst. Solids* **1985**, *75*, 63.
(14) Ruland, W. *Norelco Rep.* **1967**, *14*, 12.
(15) Ohlberg, S. M.; Alexander, L. E.; Warrick, E. L. *J. Polym. Sci.* **1958**, *27*, 1.
(16) Krimm, S.; Tobolsky, A. V. *Text. Res. J.* **1951**, *21*, 805.
(17) Murthy, N. S.; Correale, S. T.; Minor, H. *Macromolecules* **1991**, *24*, 1185.
(18) Murthy, N. S.; Correale, S. T.; Moore, R. A. F. *J. Appl. Polym. Sci., Appl. Polym. Proc.* **1991**, *47*, 185.
(19) Roldan, L. G.; Kaufman, H. S. *Polym. Lett.* **1963**, *1*, 603.
(20) Roldan, L. G.; Rahl, F.; Paterson, A. R. *J. Polym. Sci., Part C* **1965**, *8*, 145.
(21) Murthy, N. S.; Curran, S. A.; Minor, H.; Aharoni, S. M. *Macromolecules* **1991**, *24*, 3215.
(22) Murthy, N. S. *Polym. Prepr. (Am. Chem. Soc., Div. Polym. Chem.)* **1992**, *33* (1), 251.
(23) Murthy, N. S. *Polym. News* **1991**, *16*, 358.
(24) Howard, S. A. *Adv. X-ray Anal.* **1989**, *32*, 523.
(25) Murthy, N. S.; Minor, H. *Polymer* **1990**, *31*, 996.
(26) Guinier, A. *X-ray Diffraction*; Freeman: San Francisco, CA, 1963; p 73.
(27) Urbanczyk, G. W. *J. Appl. Polym. Sci.* **1989**, *38*, 55.
(28) Harget, P. J.; Oswald, H. J. *J. Polym. Sci., Polym. Phys.* **1979**, *17*, 531.
(29) Rosenfeld, Y. *Phys. Rev. A* **1990**, *42*, 5978.
(30) Hukins, D. W. L. *X-ray Diffraction by Disordered and Ordered Systems*; Pergamon: Oxford, U.K., 1981; pp 64–75.
(31) Honnell, K. G.; McCoy, J. D.; Curro, J. G.; Schweizer, K. S.; Narten, A. H.; Habenschuss, A. *J. Chem. Phys.* **1991**, *94*, 4659.
(32) Murthy, N. S.; Stamm, M.; Sibilia, J. P.; Krimm, S. *Macromolecules* **1989**, *22*, 1261.
(33) Williams, J. L.; Karam, H. J.; Cleeremen, K. J.; Rinn, H. W. *J. Polym. Sci.* **1952**, *8*, 345.
(34) Wecker, S. M.; Davidson, T.; Cohen, J. B. *J. Mater. Sci.* **1972**, *7*, 1249.
(35) Killian, H.-G.; Boueke, K. *J. Polym. Sci.* **1962**, *58*, 311.
(36) Matthews, J. L.; Peiser, H. S.; Richards, R. B. *Acta Crystallogr.* **1949**, *2*, 85.
(37) Turner-Jones, A. *J. Polym. Sci.* **1962**, *62*, S53.
(38) Read, B. E.; Stein, R. S. *Macromolecules* **1968**, *1*, 116.
(39) Murthy, N. S. *Macromolecules* **1987**, *20*, 443.
(40) Miura, H.; Hirschinger, J.; English, A. D. *Macromolecules* **1990**, *23*, 2169.
(41) Vaughan, A. S.; Ungar, G.; Bassett, D. C.; Keller, A. *Polymer* **1985**, *26*, 726.